
SAVA: Scalable Learning-Agnostic Data Valuation

Samuel Kessler *
University of Oxford
skessler@robots.ox.ac.uk

Tam Le *
The Institute of Statistical Mathematics
& RIKEN AIP
tam@ism.ac.jp

Vu Nguyen
Amazon
vutngn@amazon.com

Abstract

Selecting suitable data for training machine learning models is crucial since large, web-scraped, real datasets contain noisy artifacts that affect the quality and relevance of individual data points. These artifacts will impact the performance and generalization of the model. We formulate this problem as a data valuation task, assigning a value to data points in the training set according to how similar or dissimilar they are to a clean and curated validation set. Recently, *LAVA* (Just et al., 2023) successfully demonstrated the use of optimal transport (OT) between a large noisy training dataset and a clean validation set, to value training data efficiently, without the dependency on model performance. However, the *LAVA* algorithm requires the whole dataset as an input, this limits its application to large datasets. Inspired by the scalability of stochastic (gradient) approaches which carry out computations on *batches* of data points instead of the entire dataset, we analogously propose *SAVA*, a scalable variant of *LAVA* with its computation on batches of data points. Intuitively, *SAVA* follows the same scheme as *LAVA* which leverages the hierarchically defined OT for data valuation. However, while *LAVA* processes the whole dataset, *SAVA* divides the dataset into batches of data points, and carries out the OT problem computation on those batches. We perform extensive experiments, to demonstrate that *SAVA* can scale to large datasets with millions of data points and doesn't trade off data valuation performance.

1 Introduction

Neural scaling laws empirically show that the generalization error decreases according to a power law as the data a model trains on increases. This has been shown for natural language processing, vision, and speech (Kaplan et al., 2020; Henighan et al., 2020; Rosenfeld et al., 2019; Zhai et al., 2022; Radford et al., 2023). However, training neural networks on larger and larger datasets for moderate improvements in model accuracy is inefficient. Furthermore, production neural network models need to be continuously updated given new utterances that enter into common everyday parlance (Lazaridou et al., 2021; Baby et al., 2022). It has been shown both in theory and in practice that sub-power law, exponential scaling of model performance with dataset size is possible by carefully selecting informative data and pruning uninformative data (Sorscher et al., 2022), and that generalization improves with training speed (Lyle et al., 2020). Therefore, valuing and selecting data points that are informative: which have not been seen by the model, which do not have noisy labels, and which are relevant to the task we want to solve—are not outliers—can help to not only decrease

*equal contribution

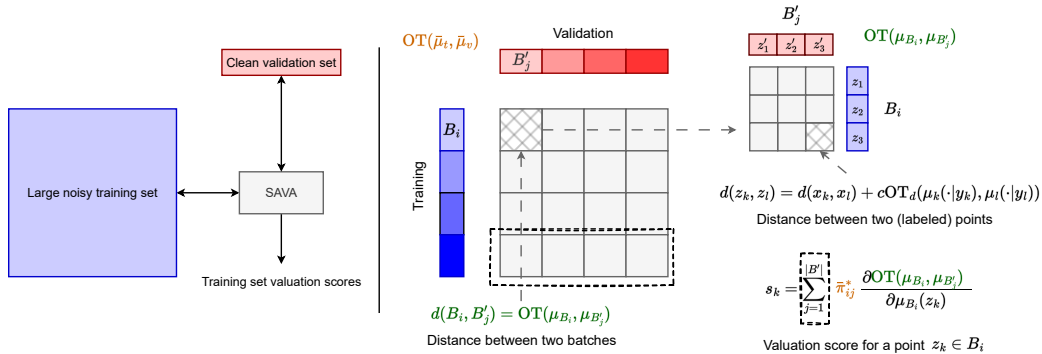


Figure 1: **Overview of the proposed SAVA method.** Instead of solving a single, but expensive, OT problem on the whole *dataset*, SAVA considers solving multiple cheaper smaller OT problems on *batches* of data points, and integrates the resulting calibrated gradients together for a data valuation task. $OT(\bar{\mu}_t, \bar{\mu}_v)$ denotes the OT cost and $\bar{\pi}^*(\bar{\mu}_t, \bar{\mu}_v)$ is its associated optimal transport plan. $OT(\mu_{B_i}, \mu_{B'_j})$ is the OT between a uniform distribution of points in the batch B_i from the training set and the batch B'_j in the validation set. s_k is SAVA’s final valuation score for training data point z_k . We provide a visualization of these artifacts generated by SAVA in Figure 12.

training times, and reduce compute costs, but also improve overall test performance (Mindermann et al., 2022; Tirumala et al., 2023).

Popular data selection and data pruning methods use variations of the model loss to value data points (Jiang et al., 2019; Pruthi et al., 2020; Paul et al., 2021). Crucially, these methods depend on the model used, and they are vulnerable to prioritizing data points with noisy labels or noisy features; data points that do not resemble the target validation set. When treating data valuation as a function of model performance, we introduce a dependency on a neural network model. This is the case when valuing a point using the leave-one-out (LOO) error, i.e., the change of model performance when the point is omitted from training. To rid our dependence on a neural network model, a promising idea is to leverage optimal transport (OT) between a training distribution and a clean validation distribution as a proxy to directly measure the value of data points in the training set in a model-agnostic fashion. In particular, the validation performance of each point in the training set can be estimated using the hierarchically defined Wasserstein between the training and the validation set (Alvarez-Melis and Fusi, 2020; Just et al., 2023). LAVA (Just et al., 2023) has been shown to successfully value data by measuring the sensitivity of the hierarchically defined Wasserstein between training data points and validation distributions in a model-agnostic fashion. However, LAVA requires significant RAM consumption since its memory complexity grows quadratically $\mathcal{O}(N^2)$ with the dataset size N . This hinders LAVA from scaling to large datasets.

In this paper, we present SAVA, a scalable variant of LAVA, for data valuation. Our method completely addresses the bottleneck of RAM requirements in LAVA. Intuitively, SAVA performs the OT computations on batches instead of on the entire dataset like LAVA (hence the analogy to the stochastic approach to gradient computation). Specifically, SAVA uses ideas from hierarchical optimal transport (Yurochkin et al., 2019; Lee et al., 2019) to enable OT calculations on batches instead of the entire dataset. We can scale up OT-based data valuation using SAVA to large real-world web-scraped datasets. On benchmark problems SAVA performs comparably to LAVA while being able to scale to datasets two orders of magnitude larger without memory issues, while LAVA is limited due to hardware memory constraints.

Contributions:

1. We introduce a novel scalable data valuation method called SAVA that leverages hierarchical optimal transport (Yurochkin et al., 2019; Lee et al., 2019) which performs OT computations on batches of data points, enabling OT-based data valuation to large datasets.
2. We provide an extensive experimental analysis to demonstrate the improved scalability with increasing dataset sizes with respect to baselines.

2 Optimal Transport for Data Valuation

2.1 Optimal Transport for Labeled Datasets

Let \mathcal{X} be the feature space, and V be the number of labels. We write $f_t : \mathcal{X} \mapsto \{0, 1\}^V$ and $f_v : \mathcal{X} \mapsto \{0, 1\}^V$ for the labeling functions for training and validation data respectively. Given the training set $\mathbb{D}_t = \{(x_i, f_t(x_i))\}_{i=1}^N$ and the validation set $\mathbb{D}_v = \{(x'_i, f_v(x'_i))\}_{i=1}^{N'}$, the corresponding measures for sets $\mathbb{D}_t, \mathbb{D}_v$ are $\mu_t(x, y) = \frac{1}{N} \sum_{i=1}^N \delta_{(x_i, y_i)}$ and $\mu_v(x', y') = \frac{1}{N'} \sum_{i=1}^{N'} \delta_{(x'_i, y'_i)}$ respectively where δ is the Dirac function, and y, y' are labels of x, x' respectively. For simplicity, let $\mathcal{Z} = (\mathcal{X}, \mathcal{Y})$ where \mathcal{Y} is the space of labels. For ease of reading, we summarize all notations in Appendix Table 1.

Following Alvarez-Melis and Fusi (2020), we compute the distance between two labels by leveraging the OT distance between the conditional distributions of the features given each label. More concretely, for label y_t in μ_t , the conditional distribution of the features given y_t in μ_t is as $\mu_t(\cdot | y_t) = \frac{\mu_t(\cdot) I[f_t(\cdot) = y_t]}{\int \mu_t(\cdot) I[f_t(\cdot) = y_t]}$, where I is the indicator function (similarly for label y_v in μ_v). Let d be the metric of the feature space \mathcal{X} , e.g., we use the Euclidean distance for d in practice. The distance between labels y_t and y_v is $\text{OT}_d(\mu_t(\cdot | y_t), \mu_v(\cdot | y_v))$, i.e., the metric of the label space \mathcal{Y} . Thus, we can compute the transport cost function between feature-label pairs in $\mathcal{Z} = (\mathcal{X}, \mathcal{Y})$ as follows

$$\mathbf{C}((x_t, y_t), (x_v, y_v)) = d(x_t, x_v) + c \text{OT}_d(\mu_t(\cdot | y_t), \mu_v(\cdot | y_v)), \quad (1)$$

where $c > 0$ is a weight coefficient. Given the cost matrix \mathbf{C} for labeled data points (i.e., feature-label points in \mathcal{Z}) in Eq. (1), we can use the OT on the represented measures μ_t, μ_v to compute the distance between the training and validation sets, i.e., $d(\mathbb{D}_t, \mathbb{D}_v)$, without relying on external models or parameters. It is worth noting that the cost matrix is hierarchically defined; it is dependent on the solution of the OT problem between labels Eq. (1). More concretely, we have

$$\text{OT}_{\mathbf{C}}(\mu_t, \mu_v) = \min_{\pi \in \Pi(\mu_t, \mu_v)} \int_{\mathcal{Z} \times \mathcal{Z}} \mathbf{C}(z, z') d\pi(z, z'), \quad (2)$$

where $\Pi(\mu_t, \mu_v)$ is the set of transportation couplings which have marginals as μ_t and μ_v . To simplify notations, we drop \mathbf{C} , and use OT when the context is clear. We further write π^* for the optimal transport plan in Eq. (2). To deal with high computational complexity, i.e., super cubic w.r.t. the number of supports of input measures, an efficient approach utilizes entropic regularization (Cuturi, 2013) to reduce its complexity into quadratic, defined as

$$\text{OT}_{\varepsilon}(\mu_t, \mu_v) = \min_{\pi \in \Pi(\mu_t, \mu_v)} \int_{\mathcal{Z} \times \mathcal{Z}} \mathbf{C}(z, z') d\pi(z, z') + \varepsilon H(\pi | \mu_t \otimes \mu_v), \quad (3)$$

where \otimes is the product measure operator, and $H(\pi | \mu_t \otimes \mu_v) = \int_{\mathcal{Z} \times \mathcal{Z}} \log\left(\frac{d\pi}{d\mu_t d\mu_v}\right) d\pi$.

Additionally, the OT problem in Eq. (2) is a constrained convex minimization, it is naturally paired with a dual problem, i.e., constrained concave maximization problem, as follows:

$$\text{OT}_{\mathbf{C}}(\mu_t, \mu_v) = \max_{(f, g) \in \mathcal{R}(\mathbf{C})} \langle f, \mu_t \rangle + \langle g, \mu_v \rangle, \quad (4)$$

where $\mathcal{R}(\mathbf{C}) = \{(f, g) \in \mathcal{C}(\mathcal{Z}) \times \mathcal{C}(\mathcal{Z}) : \forall(z, z'), f(z) + g(z') \leq \mathbf{C}(z, z')\}$, \mathcal{C} is a collection of continuous functions, and $\langle f, \mu_t \rangle = \int_{\mathcal{Z}} f(z) d\mu_t(z)$, similarly for $\langle g, \mu_v \rangle$.

2.2 LAVA: Data valuation via calibrated OT gradients

As mentioned in Just et al. (2023), the OT distance is known to be insensitive to small differences while also being not robust to large deviations. This feature is naturally suitable for detecting abnormal data points, i.e., disregarding normal variations in distances between clean data while being sensitive to abnormal distances of outlying points. Therefore, the gradient of the OT distance w.r.t. the probability mass associated with each point can be leveraged as a surrogate to measure the contribution of that point. More precisely, the gradient of the OT distance w.r.t. the probability mass of data points in the two datasets can be expressed:

$$\nabla_{\mu_t} \text{OT}(f^*, g^*) = (f^*)^T, \quad \nabla_{\mu_v} \text{OT}(f^*, g^*) = (g^*)^T. \quad (5)$$

Note that we can leverage the Sinkhorn algorithm to solve the entropic regularized OT, i.e., $\text{OT}_\varepsilon(\mu_t, \mu_v)$, and obtain the optimal dual variables (f^*, g^*) as its by-product, for computing the gradient of entropic regularized OT w.r.t. the mass of support data points of input measures.

The dual solution is unique, up to a constant due to the redundant constraint $\sum_{i=1}^N \mu_t(z_i) = \sum_{i=1}^M \mu_v(z'_i) = 1$. Therefore, for measuring the gradients of the OT w.r.t. the probability mass of a given data point in each dataset, [Just et al. \(2023\)](#) calculate the *calibrated gradients* (i.e., a sum of all elements equals to a zero vector) as

$$\frac{\partial \text{OT}(\mu_t, \mu_v)}{\partial \mu_t(z_i)} = f_i^* - \sum_{j \in \{1, \dots, N\} \setminus i} \frac{f_j^*}{N-1}, \quad (6)$$

The calibrated gradients predict how the OT distance changes as more probability mass is shifted to a given data point. This can be interpreted as a measurement of the contribution of the data point to the OT. Additionally, if we want a training set to match the distribution of the validation dataset, then either removing or reducing the mass of data points with large positive gradients, while increasing the mass of data points with large negative gradients can be expected to reduce their OT distance. Therefore, as demonstrated in [Just et al. \(2023\)](#), the calibrated gradients provide a powerful tool to detect and prune abnormal or irrelevant data in various applications.

Memory Limitation. While being used with the current best practice, the Sinkhorn algorithm for entropic regularized OT ([Cuturi, 2013](#)) still runs in quadratic memory complexity $O(N^2)$ with the dataset size N , as it requires performing operations on the entire dataset, using the full pairwise cost matrix. Consequently, the memory and RAM requirements for the Sinkhorn algorithm primarily depend on the dataset size N . Additionally, notice that a dense square (float) matrix of size $N = 10^5$ will require at least 74 GB of RAM and $N = 10^6$ will take 7450 GB of RAM which is prohibitively expensive. Therefore, *LAVA* is limited to small datasets.

Scalability. Inspired by the scalability of stochastic (gradient) approaches where the computation is carried out on batches of data points instead of the whole dataset as in the traditional gradient, we follow this simple but effective scheme to propose an analog for OT, named *SAVA* which is a scalable variant of *LAVA* with its OT computation on batches. Intuitively, *SAVA* also leverages the hierarchically defined OT as in *LAVA*, but it performs OT on batches of data points instead of on the entire dataset as in *LAVA*. We introduce *SAVA* in the next section.

It is worth noting that the OT-based data valuation we introduced in this section focuses on the *gradient* of the OT instead of the OT *distance* itself. Therefore, some popular scalable OT approaches, e.g., sliced-Wasserstein ([Rabin et al., 2011](#)), tree-sliced-Wasserstein ([Le et al., 2019](#)), or Sobolev transport ([Le et al., 2022](#)), may not be suitable to data valuation. In the next section, we introduce our novel scalable approach for computing the gradient of the OT using hierarchical OT approach ([Yurochkin et al., 2019](#); [Lee et al., 2019](#)). We focus on the problem of data valuation but our work can be readily applied for other large-scale applications where the gradient of the OT is required.

3 SAVA: Scalable Data Valuation

We present *SAVA*, a scalable data valuation method, scaling *LAVA* to a large-scale dataset. Instead of solving a single (but expensive) OT problem for distributions on the entire datasets, i.e., $\text{OT}(\mu_t, \mu_v)$ in *LAVA* with the pairwise cost matrix size $\mathbb{R}^{N \times N'}$, we consider solving multiple (cheaper) OT problems for distributions on batches of data points. For this purpose, our algorithm performs data valuation on two levels of hierarchy: across batches, and across data points within two batches. Thus, *SAVA* can complement *LAVA* for large-scale applications.

Hierarchical OT. We follow the idea in hierarchical OT approach ([Yurochkin et al., 2019](#); [Lee et al., 2019](#)) to partition the training dataset \mathbb{D}_t of N samples into K_t disjoint batches $B = \{B_i\}_{i=1}^{K_t}$. Similarly, for the validation set \mathbb{D}_v of N' samples into K_v disjoint batches $B' = \{B'_j\}_{j=1}^{K_v}$. Additionally, for all $i \in [K_t], j \in [K_v]$, let the number of samples in batches B_i, B'_j as N_i, N'_j respectively. The corresponding measures of the training and validation sets w.r.t. the batches are defined as: $\bar{\mu}_t(B) = \frac{1}{K_t} \sum_{i=1}^{K_t} \delta_{(B_i)}$ and $\bar{\mu}_v(B') = \frac{1}{K_v} \sum_{j=1}^{K_v} \delta_{(B'_j)}$ respectively. We then define a distance

Algorithm 1 Scalable Data Valuation (SAVA)

Input: a threshold τ, ϵ for Sinkhorn algorithm, let $z = (x, y)$

Output: training data values s_k for all $k \in [N_i]$ for all $i \in [K_t]$.

```

1 for  $i = 1, \dots, K_t$  do
2   for  $j = 1, \dots, K_v$  do
3     Compute  $C_{kl}(B_i, B'_j), \forall k \in [N_i], \forall l \in [N'_j]$  by using Eq. (8).
4     Compute  $f^*(\mu_{B_i}, \mu_{B'_j}), g^*(\mu_{B_i}, \mu_{B'_j})$  by solving  $\text{OT}_C(\mu_{B_i}, \mu_{B'_j})$ .
5     Set  $\bar{C}_{ij}(\bar{\mu}_t, \bar{\mu}_v) = \text{OT}_C(\mu_{B_i}, \mu_{B'_j})$ . // i.e., distance  $d(B_i, B'_j)$  on batches.
6 Compute  $\bar{\pi}^*(\bar{\mu}_t, \bar{\mu}_v) \in \mathbb{R}^{K_t \times K_v}$  by solving  $\text{OT}_{\bar{C}}(\bar{\mu}_t, \bar{\mu}_v)$ 
7 for  $i = 1, \dots, K_t$  do
8   for  $k = 1, \dots, N_i$  do
9     Compute  $\frac{\partial \text{OT}(\mu_{B_i}, \mu_{B'_j})}{\partial \mu_{B_i}(z_k)}, \forall j \in [K_v]$  using Eq. (14).
10    Compute  $s_k = \frac{\partial \text{HOT}(\mu_t, \mu_v)}{\partial \mu_t(z_l)}$  using Eq. (13). // valuation score for data point  $z_k \in B_i$ .
```

between the datasets as the hierarchical optimal transport (HOT) between the measures μ_t, μ_v as OT distance for corresponding represented measures on batches, i.e., $\bar{\mu}_t$ and $\bar{\mu}_v$ as in Sec. 2.1 as follows:

$$d(\mu_t, \mu_v) := \text{HOT}(\mu_t, \mu_v) := \text{OT}(\bar{\mu}_t, \bar{\mu}_v). \quad (7)$$

It is worth noting that HOT finds the optimal coupling at the batch level, but not at the support data point level as in the classic OT. Therefore, it can be seen that

$$\text{OT}(\mu_t, \mu_v) \leq \text{HOT}(\mu_t, \mu_v).$$

The equality happens when either each batch only has one support or each dataset only has one batch.

Our goal is to estimate the gradient $\frac{\partial d(\mu_t, \mu_v)}{\partial \mu_t(z_k)} = \frac{\partial \text{HOT}(\mu_t, \mu_v)}{\partial \mu_t(z_k)}$ where $\text{HOT}(\mu_t, \mu_v)$ is defined in the Eq. (7). Computing this derivative involves two OT estimation steps including (i) OT between individual data points within two batches to compute $d(B_i, B'_j) := \text{OT}(\mu_{B_i}, \mu_{B'_j})$, where $\mu_{B_i}, \mu_{B'_j}$ are corresponding measures for batches B_i, B'_j respectively, and subsequently a cost matrix \bar{C} on pairwise batches for input measures over batches; (ii) $d(\mu_t, \mu_v) = \text{HOT}(\mu_t, \mu_v) := \text{OT}_{\bar{C}}(\bar{\mu}_t, \bar{\mu}_v)$.

Pairwise cost between batches. We estimate the distance between two batches as the OT problem between B_i and B_j , i.e., $d(B_i, B'_j) := \text{OT}(B_i, B'_j)$ as discussed in Sec. 2.1 by viewing the OT problem between two labeled (sub)datasets or batches B_i and B'_j .

More precisely, to solve this OT problem, we calculate the pairwise cost for data points between two batches $C_{kl}(B_i, B'_j) \in \mathbb{R}^{N_i \times N'_j}$, where $\forall k \in [N_i], \forall l \in [N'_j]$, the element $C_{kl}(B_i, B'_j)$ is the cost between two labeled data points $(x_k, y_k) \in B_i$ and $(x'_l, y'_l) \in B'_j$, calculated as

$$C_{kl}(B_i, B'_j) = d(x_k, x'_l) + c \text{OT}_d(\mu_{B_i}(\cdot|y_k), \mu_{B'_j}(\cdot|y'_l)). \quad (8)$$

Given the cost matrix $C(B_i, B'_j)$, we solve $\text{OT}_C(\mu_{B_i}, \mu_{B'_j})$ to get dual solutions $f^*(\mu_{B_i}, \mu_{B'_j}), g^*(\mu_{B_i}, \mu_{B'_j})$, and the OT distance for $d(B_i, B'_j)$, i.e., $\text{OT}_C(\mu_{B_i}, \mu_{B'_j})$.

We repeat this process and solve the OT problem for each pair of (B_i, B'_j) , i.e., OT problem for distributions on batches of data points, across the training and validation datasets, i.e., for all $i \in [K_t], j \in [K_v]$. This enables us to define the cost matrix for pairwise batches in $\bar{\mu}_t, \bar{\mu}_v$, denoted as $\bar{C}(\bar{\mu}_t, \bar{\mu}_v) \in \mathbb{R}_+^{K_t \times K_v}$ where we recall that K_t and K_v are the number of batches in training and validation sets. Hence, for this cost matrix \bar{C} , the element \bar{C}_{ij} is computed as $\text{OT}(\mu_{B_i}, \mu_{B'_j})$, for all $i \in [K_t], \forall j \in [K_v]$.

Batch valuation. Given the pairwise cost matrix across batches \bar{C} , we compute the data valuation for each batch via the gradient of the distance $\text{OT}_{\bar{C}}(\bar{\mu}_t, \bar{\mu}_v)$ w.r.t. the probability mass of *batches* in the two datasets, i.e., $\frac{\partial \text{OT}_{\bar{C}}(\bar{\mu}_t, \bar{\mu}_v)}{\partial \bar{\mu}_t(B_i)}$. These partial derivatives measure the contribution of the batches to the

OT distance, i.e., shifting more probability mass to the batch would result in an increase or decrease of the dataset distance, respectively.

More precisely, let \bar{f}^*, \bar{g}^* be the optimal dual variables of $\text{OT}_{\bar{C}}(\bar{\mu}_t, \bar{\mu}_v)$, then the data valuation of the batch B_i in the training set \mathbb{D}_t is estimated as follows:

$$\frac{\partial \text{OT}_{\bar{C}}(\bar{\mu}_t, \bar{\mu}_v)}{\partial \bar{\mu}_t(B_i)} = \bar{f}_i^*. \quad (9)$$

Since the optimal dual variables are only unique up to a constant, we follow [Just et al. \(2023\)](#) to normalize these optimal dual variables such that the sum of all elements is equal to a zero vector:

$$\frac{\partial \text{OT}_{\bar{C}}(\bar{\mu}_t, \bar{\mu}_v)}{\partial \bar{\mu}_t(B_i)} = \bar{f}_i^* - \sum_{j \in \{1, \dots, K_t\} \setminus i} \frac{\bar{f}_j^*}{K_t - 1}. \quad (10)$$

Using batch valuation for data point valuation. After solving the OT problem over batches, we obtain the optimal transport plan $\bar{\pi}^*(\bar{\mu}_t, \bar{\mu}_v)$ which is used to compute the data evaluation over individual data points:

$$\bar{\pi}^*(\bar{\mu}_t, \bar{\mu}_v) = \text{diag}(\bar{f}_k^*) \exp\left(-\frac{\bar{C}(\bar{\mu}_t, \bar{\mu}_v)}{\epsilon}\right) \text{diag}(\bar{g}_k^*), \quad (11)$$

where $\text{diag}(\cdot)$ is matrix diagonal operator.

For a data point $z \in B_i \subset \mathbb{D}_t$, its data valuation score can be computed as follows:

$$\sum_{j=1}^{K_v} \bar{\pi}_{ij}^*(\bar{\mu}_t, \bar{\mu}_v) \frac{\partial \text{OT}(\mu_{B_i}, \mu_{B'_j})}{\partial \mu_{B_i}(z)}. \quad (12)$$

Using HOT, we can measure the gradients of the OT distance w.r.t. the probability mass of a given data point in each dataset via the calibrated gradient summarized in the following Lemma 1. We refer to Appendix Table 1 for the notations.

Lemma 1. *The data valuation, i.e., the calibrated gradient for a data point z_k in the batch B_i in \mathbb{D}_t can be computed as follows:*

$$\frac{\partial \text{HOT}(\mu_t, \mu_v)}{\partial \mu_t(z_k)} = \sum_{j=1}^{K_v} \bar{\pi}_{ij}^*(\bar{\mu}_t, \bar{\mu}_v) \frac{\partial \text{OT}(\mu_{B_i}, \mu_{B'_j})}{\partial \mu_{B_i}(z_k)}, \quad (13)$$

where the calibrated gradient of OT for measures on batches is calculated as follows:

$$\frac{\partial \text{OT}(\mu_{B_i}, \mu_{B'_j})}{\partial \mu_{B_i}(z_k)} = f_k^*(\mu_{B_i}, \mu_{B'_j}) - \sum_{l \in \{1, \dots, N_i\} \setminus k} \frac{f_l^*(\mu_{B_i}, \mu_{B'_j})}{N_i - 1}, \forall j \in [K_v]. \quad (14)$$

As the common practice in computing the OT via its entropic regularization, using the Sinkhorn algorithm ([Cuturi, 2013](#)), we quantify the deviation in the calibrated gradients caused by the entropy regularizer. This analysis provides foundations on the potential impact of the deviation on the applications built on these gradients.

Lemma 2. *Let $\text{HOT}(\mu_t, \mu_v)$ and $\text{OT}_{\epsilon}(\mu_t, \mu_v)$ be the HOT and entropic regularized OT between the measures μ_t and μ_v associated with the two datasets \mathbb{D}_t and \mathbb{D}_v respectively. The difference between the calibrated gradients for two data points $\{z_l, z_h\} \in B_i \subset \mathbb{D}_t$ can be calculated as*

$$\frac{\partial \text{HOT}(\mu_t, \mu_v)}{\partial \mu_t(z_k)} - \frac{\partial \text{HOT}(\mu_t, \mu_v)}{\partial \mu_t(z_l)} = \sum_{j=1}^{K_v} \bar{\pi}_{ij}^*(\bar{\mu}_t, \bar{\mu}_v) \left[\frac{\partial \text{OT}_{\epsilon}(\mu_{B_i}, \mu_{B'_j})}{\partial \mu_{B_i}(z_k)} - \frac{\partial \text{OT}_{\epsilon}(\mu_{B_i}, \mu_{B'_j})}{\partial \mu_{B_i}(z_l)} - \epsilon \frac{N_k}{N_k - 1} \left(\frac{1}{(\bar{\pi}_{\epsilon}^*)_{l,j}} - \frac{1}{(\bar{\pi}_{\epsilon}^*)_{k,j}} \right) \right]. \quad (15)$$

Proof. Refer to Appendix C for the Proof. ■



Figure 2: **SAVA can value the full CIFAR10 dataset with various corruptions, while LAVA has out-of-memory (OOM) issues.** We sort training examples by the highest OT gradients in Eq. (6) and Eq. (12) for LAVA and SAVA respectively, and use the fraction of corrupted data recovered for a prefix of size $N/4$ as the detection rate (where N is the training set size). The star symbol (\star) denotes the point at which LAVA is unable to continue valuing training due GPU out-of-memory (OOM) errors.

We make a similar observation in LAVA that the ground-truth gradient difference between two training points z_k and z_l is calculated based on the HOT formulation and can be approximated by the entropic regularized formulation OT_ϵ , such as via Sinkhorn algorithm (Cuturi, 2013). In other words, we can calculate the ground-truth difference based on the solutions to the regularized problem plus some calibration terms that scale with ϵ . In addition, in our case with HOT, the gradient difference also depends on the additional optimal assignment across batches $\tilde{\pi}^*(\bar{\mu}_t, \bar{\mu}_v)$ which is again estimated by Sinkhorn algorithm.

4 Properties and Discussions

The SAVA Algorithm. We outline the computational steps of SAVA in Algorithm 1. From Lines 1 to 5, we solve multiple OT tasks for data points between two batches B_i, B'_j . We obtain the dual solution $f^*(\mu_{B_i}, \mu_{B'_j}) \in \mathbb{R}^{N_i}$. Additionally, these OT distances are used to fill in the cost matrix for pairwise batches $\bar{C}_{ij}(\bar{\mu}_t, \bar{\mu}_v) = \text{OT}(\mu_{B_i}, \mu_{B'_j})$. Here, the cost matrix C is of size $N_i \times N'_j$ where the batch sizes $N_i, N'_j \ll N$. The required memory complexity is at least $\tilde{O}(N_i^2)$.

We then solve the OT problem across batches $\text{OT}_{\bar{C}}(\bar{\mu}_t, \bar{\mu}_v)$ to get the optimal plan $\tilde{\pi}^*(\bar{\mu}_t, \bar{\mu}_v)$ in line 6 Algorithm 1. The cost matrix is of size $K_t \times K_v$ which is typically small and so less expensive compared to the previous OT tasks. Finally, from Lines 7 to 10, we estimate valuation scores for training data using the auxiliary matrices computed in the previous steps, including $f^*(\mu_{B_i}, \mu_{B'_j})$ and $\tilde{\pi}^*(\bar{\mu}_t, \bar{\mu}_v)$.

SAVA Memory Requirements. The Sinkhorn algorithm computational complexity is at least $\tilde{O}(N^2)$ where N is the number of samples. This comes from the main OT step of $\text{OT}(\mu_t, \mu_v)$ over the full cost matrix C of size $N \times N'$ to subsequently calculate the calibrated gradient in Eq. (6) where N and N' are the training and validation dataset sizes. SAVA overcomes this limitation by solving multiple smaller OT problems $\text{OT}(\mu_{B_i}, \mu_{B'_j})$ on distributions for batches of data points only.

Practical Implementation with Caching. While yielding a significant memory improvement, SAVA’s runtime is not necessarily faster than LAVA. To speed up SAVA, we propose to implement Algorithm 1 by caching the label-to-label costs between points in the validation and training batches: $\text{OT}_d(\cdot, \cdot)$ in Eq. (1) so that it is only calculated once in the first iteration of Algorithm 1 and reused for subsequent batches. This significantly reduces SAVA runtimes with no detriment to performance Figure 9. All experimental results in Section 5, unless otherwise stated, implement this caching strategy.

Batch Sizes. If we consider Eq. (7), HOT provides the upper bound for the OT since its optimal coupling is on batches of data points. HOT recovers the OT when either batch only has one support or each dataset only has one batch. Consequently, up to a certain batch size, when increasing the batch size N_i , HOT converges to the OT, but its memory complexity also increases, i.e., $\mathcal{O}(N_i^2) \rightarrow \mathcal{O}(N^2)$. On the other hand, if the batch size N_i is too small, the number of batches K_t will be large. As a result, the memory complexity will also be high (i.e., for solving $\text{OT}_{\bar{C}}(\bar{\mu}_t, \bar{\mu}_v)$ in Algorithm 1). Thus, the batch size will trade off the memory complexity and the approximation of HOT to OT.

5 Experiments

We aim to test two following hypotheses²:

1. Can *SAVA* scale and overcome the memory complexity issues which hinder *LAVA*?
2. Can *SAVA* scale to a large real-world noisy dataset with over a *million* data points?

5.1 Dataset Corruption Detection

We test the scalability of *SAVA* versus *LAVA* (Just et al., 2023) by leveraging the CIFAR10 dataset, introducing a corruption to a percentage of the training data, but keeping the validation set clean. We then assign a value to each data point in the training set. Following Pruthi et al. (2020); Just et al. (2023), we sort the training examples by their values. An effective data valuation method would rank corrupted examples in a prefix of ordered points. We use the fraction of corrupted data recovered by the prefix of size $N/4$ as our detection rate (see an example in Appendix E, Figure 6).

Setup. We consider 4 different corruptions (see Appendix D for details) that are applied to the training data following the settings in Just et al. (2023): (i) *noisy labels*, (ii) *noisy features*, (iii) *backdoor attacks* and (iv) *poison detections*. All experiments are run on a Tesla K80 Nvidia GPUs with 12GB GPU RAM. Unless otherwise stated, all results reported are a mean ± 1 standard deviation over 5 independent runs.

Baselines. Our main baseline is *LAVA* which shares the same design scheme based on hierarchically defined OT for data valuation Eq. (1). For *SAVA* and *LAVA* we use features from a pre-trained ResNet18 (He et al., 2016). For *SAVA*, we use a default batch size of $N_i = 1024$ which is its main hyperparameter.³ We also consider *KNN Shapley* (Jia et al., 2019a), the Shapley value measures the marginal improvement in the utility of a data point and uses KNN to approximate the Shapley value. *KNN Shapley* also uses ResNet18 features to calculate Shapley values, we tune k as its performance is sensitive to this hyperparameter. We also consider *TracInCP* (Pruthi et al., 2020) which measures the influence of each training point by measuring the difference in the loss at the beginning versus the end of training (see Appendix F.1 for details). We also compare with *Influence Function* (Koh and Liang, 2017) which approximates the effect of holding out a training point on the test error, it uses expensive approximations of the Hessian to calculate the influence of a training point. We finally consider a naive OT baseline which obtains values for data points at a batch level, and aggregates values across validation batches; the baseline essentially performs *LAVA* only at a data point level within a batch without a batch level OT problem, line 6 Algorithm 1. We call this baseline *Batch-wise LAVA*. Although *Batch-wise LAVA* obtains good corruption detection results, it is very sensitive to the batch size (see Appendix G).

Noisy labels. We corrupt 30% of the labels in the training set by randomly assigning the target a different label. From Figure 2, we can see that *LAVA* has an out-of-memory (OOM) issue when valuing the full training set of 50K points. In contrast, *SAVA*, *Batch-wise LAVA* *KNN Shapley* can consistently value and detect all corruptions when inspecting 12.5K ordered samples by values. *Influence Functions* matches the performance of *SAVA*, but is very expensive to run on large datasets. *TracInCP* is unable to detect noisy labels better than random selection, similar to the observations in Just et al. (2023). Consequently, when pruning 30% of the data, *SAVA* can consistently improve its accuracy on the test set as the training set size increases (Figure 3).

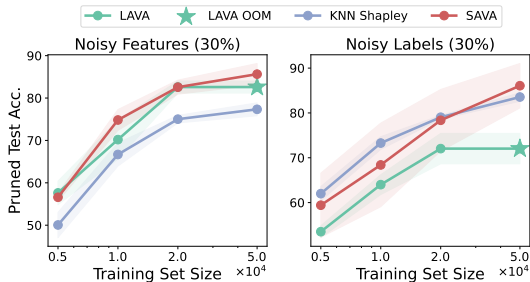


Figure 3: **SAVA can scale to the full CIFAR10 dataset enabling better data selection performance.** After valuation, we prune a prefix of size $N/4$ and train a ResNet18 model on the remaining points to report test accuracy. The symbol (★) denotes the point at which *LAVA* is unable to continue valuing training due to GPU out-of-memory (OOM) errors.

²The code to reproduce all experiments can be found at <https://github.com/skezle/sava>.

³See Appendix G for the study of the sensitivity of the batch size N_i in *SAVA*.

Noisy features. We add Gaussian noise to 30% of the training images to simulate feature corruptions that might occur in real datasets. From Figure 2, *LAVA* obtains good performance for moderate dataset sizes, but for training set sizes above 10K, some runs have OOM errors when embedding the entire training set into memory and when calculating the full cost matrix for OT problem in Eq. (1). In contrast, *SAVA* can consistently value and detect corruptions. *Batch-wise LAVA* is also able to scale and gets similar performance to *SAVA*. As can *KNN Shapley*, albeit its detection rate is lower than *SAVA*. *TracInCP* and *Influence Functions* both struggle to detect noisy data points, both methods were originally shown to detect noisy labels, so we do not expect them to work well beyond noisy label detection.

Backdoor attacks. We corrupt 10% of the data with a Trojan square attack (Liu et al., 2018). *SAVA*, *Batch-wise LAVA* and *KNN Shapley* can scale as the dataset size increases while *LAVA* has an OOM error when valuing the largest dataset with 50k points. *TracInCP* and *Influence Functions* both struggle to detect backdoored training points and have long runtimes.

Poisoning attacks. We corrupt 10% of the data with a poison frogs attack (Shafahi et al., 2018). We find in Figure 2 that *SAVA* and *Batch-wise LAVA* can scale and maintain a high detection rate. In contrast, *KNN Shapley* struggles to detect many corrupted data points after inspecting 25% of the ordered training data. Both *TracInCP* and *Influence Functions* struggle to detect the corrupted data.

Pruning. We can prune the $N/4$ data points and train a classifier on the pruned dataset in Figure 3. *SAVA* can value a larger and larger pool of training data. The subsequently pruned dataset provides better and better performance as more clean data - which resembles the validation set - is used for training. In contrast, *LAVA* has an OOM issue for the largest dataset when running the Sinkhorn algorithm on a training set of size 50K. As a result, the performance of the ResNet18 model does not improve when valuing larger training sets with *LAVA*.

5.2 Large Scale Valuation and Pruning

We test our second hypothesis: whether *SAVA* can scale to a large real-world dataset. We consider the web-scraped dataset Clothing1M (Xiao et al., 2015) where the training set has over 1M images whose labels are noisy and unreliable. However, the validation set has been curated. Clothing1M is a 14-way image classification problem and has been used for previous work on online data selection (Mindermann et al., 2022). We consider *SAVA* and other data pruning methods as baselines to remove low-value training data points before training a ResNet18 classifier.

We compare to *Batch-wise LAVA*, introduced in Section 5.1. We also compare to *EL2N* (Paul et al., 2021) which values training points using the loss on several partially trained networks to decide which points to remove. We train 10 models for 10 epochs, we perform a cross-validate a sliding window of values to decide which *EL2N* values to keep (see Appendix F.2.2 for details). We also consider supervised prototypes (Sorscher et al., 2022) which prunes image embeddings according to how similar they look to cluster centers after clustering image embeddings (see Appendix F.2.3 for details).

If we were to train a classifier on the full noisy training set, we would obtain an accuracy of 67.6 ± 0.2 , this remains constant as we randomly prune more data. Supervised prototypes obtains better results than random, and improves slightly over random pruning. This is expected since supervised prototypes is a semantic deduplication method and ignores label information. *SAVA*, *Batch-wise LAVA* and *EL2N* perform well and we find that *SAVA* performs better than both *EL2N* and *Batch-wise LAVA*. This shows the benefit of the *SAVA*'s weighting of the gradient of the OT across the validation dataset using optimal plan across batches $\bar{\pi}^*(\bar{\mu}_t, \bar{\mu}_v)$ rather than *Batch-wise LAVA*'s uniform weighting. *SAVA* produces the best accuracy model of 70.0 ± 0.2 in Figure 4.

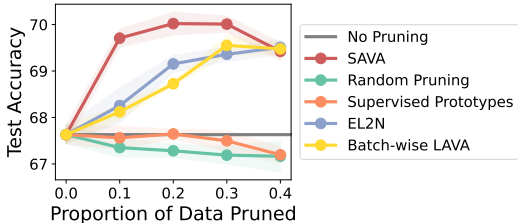


Figure 4: **SAVA can scale to a large web-scraped dataset.** We use *SAVA* and other baselines, to value data points in the noisy training set and then prune a certain percentage of the dataset. The resulting dataset is used for training a classifier.

6 Conclusions

We have presented a scalable extension to *LAVA* to address the challenges posed by large-scale datasets. Instead of relying on the expensive OT computation on the whole dataset, our proposed *SAVA* algorithm involves jointly optimizing multiple smaller OT tasks across batches of data points and within those individual batches. We empirically show that *SAVA* maintains performance in data valuation tasks while successfully scaling up to handle a large real-world noisy dataset. This makes the data valuation task feasible for large-scale datasets.

Limitations. HOT finds the optimal coupling at the batch level, but not at the global level as in the traditional OT, i.e., $OT(\mu_t, \mu_v) \leq HOT(\mu_t, \mu_v)$, which makes the validation error bound looser (Just et al., 2023, Eq. (1), Theorem 1). However, our experiments indicate little performance degradation for small datasets between *SAVA* and *LAVA*. See Appendix B for further discussion on limitations.

7 Acknowledgements

The authors would like to thank Hoang Anh Just for helpful discussions. TL acknowledges the support of JSPS KAKENHI Grant number 23K11243, and Mitsui Knowledge Industry Co., Ltd. grant.

References

- Abbas, A., Tirumala, K., Simig, D., Ganguli, S., and Morcos, A. S. (2023). Semdedup: Data-efficient learning at web-scale through semantic deduplication. *arXiv preprint arXiv:2303.09540*. 21
- Alvarez-Melis, D. and Fusi, N. (2020). Geometric dataset distances via optimal transport. *Advances in Neural Information Processing Systems*, 33:21428–21439. 2, 3
- Baby, D., D’Alterio, P., and Mendelev, V. (2022). Incremental learning for rnn-transducer based speech recognition models. 1, 17
- Coleman, C., Yeh, C., Mussmann, S., Mirzasoleiman, B., Bailis, P., Liang, P., Leskovec, J., and Zaharia, M. (2019). Selection via proxy: Efficient data selection for deep learning. In *International Conference on Learning Representations*. 19
- Cuturi, M. (2013). Sinkhorn distances: Lightspeed computation of optimal transport. In *Advances in Neural Information Processing Systems*, pages 2292–2300. 3, 4, 6, 7
- Freund, Y., Seung, H. S., Shamir, E., and Tishby, N. (1997). Selective sampling using the query by committee algorithm. *Machine learning*, 28:133–168. 19
- Gal, Y., Islam, R., and Ghahramani, Z. (2017). Deep bayesian active learning with image data. In *International Conference on Machine Learning*, pages 1183–1192. PMLR. 19
- Ghorbani, A. and Zou, J. (2019). Data shapley: Equitable valuation of data for machine learning. In *International Conference on Machine Learning*, pages 2242–2251. PMLR. 19
- He, K., Zhang, X., Ren, S., and Sun, J. (2016). Deep residual learning for image recognition. In *Proceedings of the IEEE conference on computer vision and pattern recognition*, pages 770–778. 8, 17
- Henighan, T., Kaplan, J., Katz, M., Chen, M., Hesse, C., Jackson, J., Jun, H., Brown, T. B., Dhariwal, P., Gray, S., et al. (2020). Scaling laws for autoregressive generative modeling. *arXiv preprint arXiv:2010.14701*. 1
- Houlsby, N., Huszár, F., Ghahramani, Z., and Lengyel, M. (2011). Bayesian active learning for classification and preference learning. *arXiv preprint arXiv:1112.5745*. 19
- Jia, R., Dao, D., Wang, B., Hubis, F. A., Gürel, N. M., Li, B., Zhang, C., Spanos, C. J., and Song, D. (2019a). Efficient task-specific data valuation for nearest neighbor algorithms. *Proceedings of the VLDB Endowment*, 12(11):1610–1623. 8, 19
- Jia, R., Dao, D., Wang, B., Hubis, F. A., Hynes, N., Gürel, N. M., Li, B., Zhang, C., Song, D., and Spanos, C. J. (2019b). Towards efficient data valuation based on the shapley value. In *The 22nd International Conference on Artificial Intelligence and Statistics*, pages 1167–1176. PMLR. 19

- Jiang, A. H., Wong, D. L.-K., Zhou, G., Andersen, D. G., Dean, J., Ganger, G. R., Joshi, G., Kaminsky, M., Kozuch, M., Lipton, Z. C., et al. (2019). Accelerating deep learning by focusing on the biggest losers. *arXiv preprint arXiv:1910.00762*. 2
- Jiang, K. F., Liang, W., Zou, J., and Kwon, Y. (2023). Opendataval: a unified benchmark for data valuation. 19
- Johnson, T. B. and Guestrin, C. (2018). Training deep models faster with robust, approximate importance sampling. *Advances in Neural Information Processing Systems*, 31. 21
- Just, H. A., Kang, F., Wang, T., Zeng, Y., Ko, M., Jin, M., and Jia, R. (2023). Lava: Data valuation without pre-specified learning algorithms. In *International Conference on Learning Representations*. 1, 2, 3, 4, 6, 8, 10, 13, 14, 17, 19, 21
- Kaplan, J., McCandlish, S., Henighan, T., Brown, T. B., Chess, B., Child, R., Gray, S., Radford, A., Wu, J., and Amodei, D. (2020). Scaling laws for neural language models. *arXiv preprint arXiv:2001.08361*. 1
- Katharopoulos, A. and Fleuret, F. (2018). Not all samples are created equal: Deep learning with importance sampling. In *International Conference on Machine Learning*, pages 2525–2534. PMLR. 21
- Kirsch, A., Van Amersfoort, J., and Gal, Y. (2019). Batchbald: Efficient and diverse batch acquisition for deep bayesian active learning. *Advances in Neural Information Processing Systems*, 32. 19
- Koh, P. W. and Liang, P. (2017). Understanding black-box predictions via influence functions. In *International Conference on Machine Learning*, pages 1885–1894. PMLR. 8, 19
- Kwon, Y. and Zou, J. (2022). Beta shapley: a unified and noise-reduced data valuation framework for machine learning. In *International Conference on AI and Statistics*. 19
- Lazaridou, A., Kuncoro, A., Gribovskaya, E., Agrawal, D., Liska, A., Terzi, T., Gimenez, M., de Masson d’Autume, C., Kocisky, T., Ruder, S., et al. (2021). Mind the gap: Assessing temporal generalization in neural language models. *Advances in Neural Information Processing Systems*, 34:29348–29363. 1
- Le, T., Nguyen, T., Phung, D., and Nguyen, V. A. (2022). Sobolev transport: A scalable metric for probability measures with graph metrics. In *International Conference on Artificial Intelligence and Statistics*, pages 9844–9868. PMLR. 4
- Le, T., Yamada, M., Fukumizu, K., and Cuturi, M. (2019). Tree-sliced variants of Wasserstein distances. In *Advances in neural information processing systems*, pages 12283–12294. 4
- Lee, J., Dabagia, M., Dyer, E., and Rozell, C. (2019). Hierarchical optimal transport for multimodal distribution alignment. *Advances in Neural Information Processing Systems*, 32. 2, 4, 13
- Li, M. and Sethi, I. K. (2006). Confidence-based active learning. *IEEE Transactions on Pattern Analysis and Machine Intelligence*, 28(8):1251–1261. 19
- Liu, Y., Ma, S., Aafer, Y., Lee, W.-C., Zhai, J., Wang, W., and Zhang, X. (2018). Trojaning attack on neural networks. In *25th Annual Network And Distributed System Security Symposium (NDSS 2018)*. Internet Soc. 9, 15
- Loshchilov, I. and Hutter, F. (2015). Online batch selection for faster training of neural networks. *arXiv preprint arXiv:1511.06343*. 21
- Lyle, C., Schut, L., Ru, R., Gal, Y., and van der Wilk, M. (2020). A bayesian perspective on training speed and model selection. *Advances in Neural Information Processing Systems*, 33:10396–10408. 1
- Mindermann, S., Brauner, J. M., Razzak, M. T., Sharma, M., Kirsch, A., Xu, W., Höltingen, B., Gomez, A. N., Morisot, A., Farquhar, S., et al. (2022). Prioritized training on points that are learnable, worth learning, and not yet learnt. In *International Conference on Machine Learning*, pages 15630–15649. PMLR. 2, 9, 21
- Mirzasoleiman, B., Bilmes, J., and Leskovec, J. (2020). Coresets for data-efficient training of machine learning models. In *International Conference on Machine Learning*, pages 6950–6960. PMLR. 19
- Park, D., Papailiopoulos, D., and Lee, K. (2022). Active learning is a strong baseline for data subset selection. In *Has it Trained Yet? NeurIPS 2022 Workshop*. 19

- Paul, M., Ganguli, S., and Dziugaite, G. K. (2021). Deep learning on a data diet: Finding important examples early in training. *Advances in Neural Information Processing Systems*, 34:20596–20607. [2](#), [9](#), [16](#), [21](#)
- Peyré, G. and Cuturi, M. (2019). Computational optimal transport. *Foundations and Trends® in Machine Learning*, 11(5-6):355–607. [21](#)
- Pruthi, G., Liu, F., Kale, S., and Sundararajan, M. (2020). Estimating training data influence by tracing gradient descent. *Advances in Neural Information Processing Systems*, 33:19920–19930. [2](#), [8](#), [15](#), [19](#)
- Rabin, J., Peyré, G., Delon, J., and Bernot, M. (2011). Wasserstein barycenter and its application to texture mixing. In *International Conference on Scale Space and Variational Methods in Computer Vision*, pages 435–446. [4](#)
- Radford, A., Kim, J. W., Xu, T., Brockman, G., McLeavey, C., and Sutskever, I. (2023). Robust speech recognition via large-scale weak supervision. In *International Conference on Machine Learning*, pages 28492–28518. PMLR. [1](#), [14](#)
- Ren, M., Zeng, W., Yang, B., and Urtasun, R. (2018). Learning to reweight examples for robust deep learning. In *International Conference on Machine Learning*, pages 4334–4343. PMLR. [21](#)
- Rosenfeld, J. S., Rosenfeld, A., Belinkov, Y., and Shavit, N. (2019). A constructive prediction of the generalization error across scales. In *International Conference on Learning Representations*. [1](#)
- Sener, O. and Savarese, S. (2018). Active learning for convolutional neural networks: A core-set approach. In *International Conference on Learning Representations*. [19](#)
- Settles, B. (2009). Active learning literature survey. [19](#)
- Shafahi, A., Huang, W. R., Najibi, M., Suci, O., Studer, C., Dumitras, T., and Goldstein, T. (2018). Poison frogs! targeted clean-label poisoning attacks on neural networks. *Advances in Neural Information Processing Systems*, 31. [9](#), [15](#)
- Sorscher, B., Geirhos, R., Shekhar, S., Ganguli, S., and Morcos, A. (2022). Beyond neural scaling laws: beating power law scaling via data pruning. *Advances in Neural Information Processing Systems*, 35:19523–19536. [1](#), [9](#), [21](#)
- Tirumala, K., Simig, D., Aghajanyan, A., and Morcos, A. S. (2023). D4: Improving llm pretraining via document de-duplication and diversification. In *Thirty-seventh Conference on Neural Information Processing Systems Datasets and Benchmarks Track*. [2](#), [21](#)
- Toneva, M., Sordani, A., des Combes, R. T., Trischler, A., Bengio, Y., and Gordon, G. J. (2018). An empirical study of example forgetting during deep neural network learning. [21](#)
- Wang, T. and Jia, R. (2022). Data banzhaf: A data valuation framework with maximal robustness to learning stochasticity. *arXiv preprint arXiv:2205.15466*. [19](#)
- Wu, Z., Shu, Y., and Low, B. K. H. (2022). Davinz: Data valuation using deep neural networks at initialization. In *International Conference on Machine Learning*, pages 24150–24176. PMLR. [19](#)
- Xiao, T., Xia, T., Yang, Y., Huang, C., and Wang, X. (2015). Learning from massive noisy labeled data for image classification. In *Proceedings of the IEEE Conference on Computer Vision and Pattern Recognition*, pages 2691–2699. [9](#), [14](#)
- Xie, S. M., Santurkar, S., Ma, T., and Liang, P. S. (2023). Data selection for language models via importance resampling. *Advances in Neural Information Processing Systems*, 36:34201–34227. [21](#)
- Xu, X., Wu, Z., Foo, C. S., and Low, B. K. H. (2021). Validation free and replication robust volume-based data valuation. *Advances in Neural Information Processing Systems*, 34:10837–10848. [19](#)
- Yan, T. and Procaccia, A. D. (2021). If you like shapley then you’ll love the core. In *Proceedings of the AAAI Conference on Artificial Intelligence*, volume 35, pages 5751–5759. [19](#)
- Yurochkin, M., Claiici, S., Chien, E., Mirzazadeh, F., and Solomon, J. M. (2019). Hierarchical optimal transport for document representation. *Advances in Neural Information Processing Systems*, 32. [2](#), [4](#), [13](#)
- Zhai, X., Kolesnikov, A., Houlsby, N., and Beyer, L. (2022). Scaling vision transformers. In *Proceedings of the IEEE/CVF Conference on Computer Vision and Pattern Recognition*, pages 12104–12113. [1](#)

Variable	Definition
$z = (x, y) \in \mathbb{R}^{ \mathcal{X} } \times \{0, 1\}^V$	Datapoint feature and label where V is #label and \mathcal{X} is a feature space.
$\mathbb{D}_t, \mathbb{D}_v$	Datasets for training $\mathbb{D}_t = \{(x_i, f_t(x_i))\}_{i=1}^N$ and validation $\mathbb{D}_v = \{(x'_i, f_v(x'_i))\}_{i=1}^{N'}$.
$B = \{B_i\}_{i=1}^{K_t}, B' = \{B'_j\}_{j=1}^{K_v}$	Disjoined batches for \mathbb{D}_t and \mathbb{D}_v where K_t, K_v are the number of batches.
$B_i = \{z_k\}_{k=1}^{N_i}$	Batch of datapoints where N_i is the number of datapoints in the batch i .
$\mu_{B_i} = \frac{1}{N_i} \sum_{t=1}^{N_i} \delta_{(z_t)}$	Measure over labeled datapoints for the batch B_i .
$\mu_t(x, y) = \frac{1}{N} \sum_{i=1}^N \delta_{(x_i, y_i)}$	Measure over training set.
$\mu_v(x, y) = \frac{1}{N'} \sum_{i=1}^{N'} \delta_{(x_i, y_i)}$	Measure over validation set.
$\bar{\mu}_t = \frac{1}{K_t} \sum_{i=1}^{K_t} \delta_{(B_i)}$	Measure over batches for the training set.
$\bar{\mu}_v = \frac{1}{K_v} \sum_{j=1}^{K_v} \delta_{(B'_j)}$	Measure over batches for the validation set.
$\bar{C} \in \mathbb{R}_+^{K_t \times K_v}$	Cost matrix over <i>batches</i> , each element $\bar{C}_{i,j} = d(B_i, B'_j)$.
$C \in \mathbb{R}_+^{N_i \times N'_j}$	Cost matrix over <i>labeled datapoints</i> within batches B_i and B'_j , each element $C_{kl} = d(z_k, z'_l)$.
$f^* \in \mathbb{R}^{N_i}, g^* \in \mathbb{R}^{N'_j}$	Dual solutions of the OT over a cost matrix $C \in \mathbb{R}^{N_i \times N'_j}$.
$\pi^* \in \mathbb{R}^{N_i \times N'_j}$	OT plan over a cost matrix $C \in \mathbb{R}^{N_i \times N'_j}$.
$\bar{f}^* \in \mathbb{R}^{K_t}, \bar{g}^* \in \mathbb{R}^{K_v}$	OT dual solutions over a cost matrix over batches $\bar{C} \in \mathbb{R}^{K_t \times K_v}$.
$\bar{\pi}^* \in \mathbb{R}^{K_t \times K_v}$	OT plan over a cost matrix between batches $\bar{C} \in \mathbb{R}^{K_t \times K_v}$.

Table 1: Notations used throughout the paper. We use column vectors in all notations.

Appendix

In this appendix, we provide discussion regarding the border impact of our work in §A and the limitations of our work in §B. We also provide details of theoretical results in §C, describe the data corruptions used in our experiments in §D. In §E, we further discuss how we calculate detection rates and discuss data valuation rankings. We also give details for the implementations used in the experiments in §F. In §G, we provide further empirical results. In §H, we present and discuss further related works. We also provide a visualization for the artifacts in SAVA in §I, and other further discussions in §J.

Appendix A Broader Impact

Data selection in deep learning for training neural networks can significantly enhance the efficiency and effectiveness of model training. By enabling faster training and improved generalization performance, data selection techniques reduce the computational resources and time required, leading to notable environmental benefits such as lower energy consumption and reduced carbon footprint. By using, an optimal transport approach to data valuation ensures high-quality, relevant data is selected, improving model performance. However, this approach also carries risks: a malicious actor could curate a harmful validation dataset, leading to the training of models on dangerous or unethical data. This underscores the importance of vigilance and ethical considerations in dataset creation and curation.

Appendix B Limitations

One theoretical limitation, stated in Section 6 regards a looser validation error bound (Just et al., 2023, Eq. (1), Theorem 1) due to the use of hierarchical optimal transport (Yurochkin et al., 2019; Lee et al., 2019). However, the validation error bound for SAVA remains useful as in LAVA since it can be interpreted that minimizing either the OT or hierarchical OT between training and validation sets, and will bound the model’s validation error. As we observe in practice, there is little difference in performance between SAVA and LAVA (Just et al., 2023).



Figure 5: **Examples of the data corruptions used in our experimental setup.** Examples of data from the CIFAR10 dataset where the images have corruptions: noisy features, trojan square, and poison frogs corruptions respectively.

Another limitation of our work is that the ground cost we consider Equation (1) is limited to labeled datasets.⁴ We have not explored different ground truth costs for text data or speech data.

Appendix C Details of Theoretical Results

We present the Proof of Lemma 2 as follows.

Lemma 3 (restated). *Let $\text{HOT}(\mu_t, \mu_v)$ and $\text{OT}_\epsilon(\mu_t, \mu_v)$ be the HOT and entropic regularized OT between the empirical measures μ_t and μ_v associated with the two datasets \mathbb{D}_t and \mathbb{D}_v respectively. The difference between the calibrated gradients for two datapoints $\{z_l, z_h\} \in B_i \subset \mathbb{D}_t$ can be calculated as*

$$\begin{aligned} & \frac{\partial \text{HOT}(\mu_t, \mu_v)}{\partial \mu_t(z_k)} - \frac{\partial \text{HOT}(\mu_t, \mu_v)}{\partial \mu_t(z_l)} \\ &= \sum_{j=1}^{K_v} \bar{\pi}_{ij}^*(\bar{\mu}_t, \bar{\mu}_v) \left[\frac{\partial \text{OT}_\epsilon(\mu_{B_i}, \mu_{B_j'})}{\partial \mu_{B_i}(z_k)} - \frac{\partial \text{OT}_\epsilon(\mu_{B_i}, \mu_{B_j'})}{\partial \mu_{B_i}(z_l)} - \epsilon \frac{N_k}{N_k - 1} \left(\frac{1}{(\bar{\pi}_\epsilon^*)_{l,j}} - \frac{1}{(\bar{\pi}_\epsilon^*)_{k,j}} \right) \right]. \end{aligned} \quad (\text{C.1})$$

Proof. Let $\text{OT}(\mu_t, \mu_v)$ be the OT formulation between empirical measures μ_t and μ_v , we present the proof as follows

$$\begin{aligned} & \frac{\partial \text{HOT}(\mu_t, \mu_v)}{\partial \mu_t(z_k)} - \frac{\partial \text{HOT}(\mu_t, \mu_v)}{\partial \mu_t(z_l)} \\ &= \sum_{j=1}^{K_v} \bar{\pi}_{ij}^*(\bar{\mu}_t, \bar{\mu}_v) \left[\frac{\partial \text{OT}(\mu_{B_i}, \mu_{B_j'})}{\partial \mu_{B_i}(z_k)} - \frac{\partial \text{OT}(\mu_{B_i}, \mu_{B_j'})}{\partial \mu_{B_i}(z_l)} \right] \end{aligned} \quad (\text{C.2})$$

$$= \sum_{j=1}^{K_v} \bar{\pi}_{ij}^*(\bar{\mu}_t, \bar{\mu}_v) \left[\frac{\partial \text{OT}_\epsilon(\mu_{B_i}, \mu_{B_j'})}{\partial \mu_{B_i}(z_k)} - \frac{\partial \text{OT}_\epsilon(\mu_{B_i}, \mu_{B_j'})}{\partial \mu_{B_i}(z_l)} - \epsilon \frac{N_i}{N_i - 1} \left(\frac{1}{(\bar{\pi}_\epsilon^*)_{l,j}} - \frac{1}{(\bar{\pi}_\epsilon^*)_{k,j}} \right) \right] \quad (\text{C.3})$$

where Eq.(C.2) follows the definition of HOT and Eq. (C.3) utilizes Theorem 2 in Just et al. (2023). \blacksquare

Appendix D Data Corruptions Descriptions

We consider 4 different corruptions in our experiments (Section 5) that are applied to the training set following the settings in Just et al. (2023):

Noisy labels. We corrupt a proportion of the labels in the training set by randomly assigning the target a different label. This is a common corruption found in webscale vision (Xiao et al., 2015) and speech (Radford et al., 2023) for instance.

Noisy features. We add Gaussian noise to a certain proportion of the images in the training set to simulate common background noise corruptions that might occur in real datasets.

⁴For unlabelled datasets, in some sense, it is equivalent to set the weight coefficient $c = 0$, to ignore the contribution of label information for the ground cost.

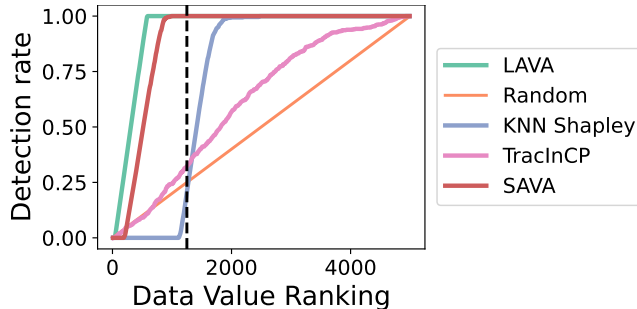


Figure 6: Data value rankings for various methods for the 10% poison frogs corruption. The number of corrupt datapoints in the prefix determines the detection rate. The black dashed line represents the $N/4$ prefix which is used for calculating the detection rates in Figure 2 and Figure 3.

Backdoor attacks. A certain proportion of the training set is corrupted with a Trojan square attack Liu et al. (2018), e.g., corrupted images have 10×10 pixel square trigger mask added with random noise and are relabeled to the trojan “airplane” class, see Figure 5 for an example of a corrupted image.

Poison detections A certain proportion of training data from a specific base class is poisoned such that the features look similar to a target class (Shafahi et al., 2018). Our target is the cat class from the CIFAR10 dataset, which is a randomly chosen image of a cat from the test set. We take a certain percentage of the base class which, in our case is the frog class from the CIFAR10 training dataset. Then we optimize the poisoned images themselves using gradient descent such that the feature spaces are close in Euclidean distance to the target cat image’s features using a pre-trained feature extractor model (in our case a pre-trained ResNet18 model). This means that the poisoned images contain features that look like the cat class and the labels are kept the same, meaning that this is a very difficult attack to detect, and the features of frogs are poisoned to look like cats and labels remain uncorrupted. See Figure 5 for an example of a poisoned frog image.

Appendix E Data Valuation Rankings

Corrupt data points are likely to be assigned a high value (a low value for KNN Shapley) and so can be used for ranking the data by importance. Therefore, following Pruthi et al. (2020), we sort the training examples by their value in descending order (ascending order for KNN Shapley). An effective data valuation method would rank corrupted examples toward the start of the data valuation ranking. We use the fraction of corrupted data recovered by the prefix of size $N/4$ as our detection rate to measure the effectiveness of various methods in Figure 2. See Figure 6 for an example of this using a poison frogs (Shafahi et al., 2018) corruption on 10% of a dataset of size 5k on CIFAR10.

Appendix F Implementation Details

F.1 CIFAR10 Corruption Detection

We use a single Nvidia K80 GPU to run all experiments.

TraInCP. In practice, TraInCP measures the influence of a training point by the dot product of the gradient of the NN model parameters evaluated on the validation set and the gradient of the NN model parameters evaluated on the specific training points, summed throughout training using saved checkpoints of a ResNet18 model trained for 100 epochs and achieves a test accuracy of 83% and training accuracy of 99%. We calculate gradients over the entire model and use every second checkpoint to calculate TraInCP values, these design choices result in fewer approximations than the original implementation (Pruthi et al., 2020).

Influence Functions. We use the following repository for obtaining results on influence functions with default parameters https://github.com/nimarb/pytorch_influence_functions.

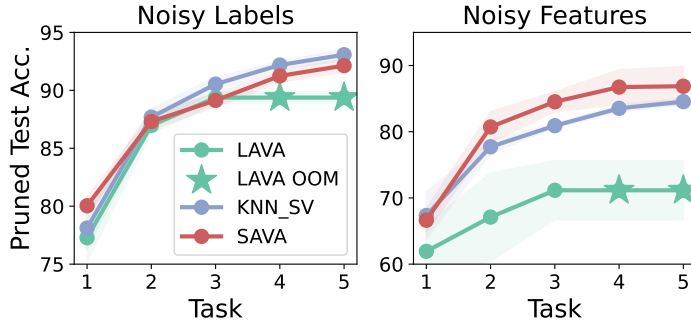


Figure 7: **SAVA can value more data as a dataset incrementally increases in size.** For each task, we value the data and prune 30% of the data which we then train a CNN to obtain a test accuracy. Left: 30% noisy labels setting. Right: 30% noisy feature setting. The star symbol (★) denotes the point at which *LAVA* is unable to continue valuing training due GPU out-of-memory errors.

KNN Shapley. The method is very sensitive to k which is a hyperparameter in the KNN algorithm used to approximate the expensive calculation of the Shapley value. We do a grid search over $k \in \{5, 10, 20, 50, 100, 200, 500, 1,000, 2,000\}$ on a validation set of size 1,000 and training set of size 2,000, where the validation set is taken from the CIFAR10 training set. Our implementation is the same as that used in the *LAVA*.

Pruning. For the pruning experiments we greedily prune $N/4$ of the ranked points with the lowest value; the highest gradient of the OT for *SAVA* and *LAVA*. We then train a ResNet18 with the SGD optimizer with weight decay of 5×10^{-4} and momentum of 0.9 for 200 epochs with a learning rate schedule where for the first 100 epochs the learning rate is 0.1, then for the next 50 epochs the learning rate is 0.01, then the final 50 epochs the learning rate is 0.001.

F.2 Clothing1M

For all experiments, we use a node with 8 Nvidia K80 GPUs.

We use a ResNet18 model for feature extraction and for obtaining a final performance metric. We use an Adam optimizer with a weight decay of 0.002. Since the pruned datasets can be of different sizes depending on the amount of pruning. We train for a fixed number of 100k steps. We use a learning rate schedule where for the first 30k steps the learning rate is 0.1 then the next 30k steps the learning rate is 0.05 then the next 20k steps the learning rate is 0.01, then the next 10k steps the learning rate is 0.001, then the next 5k steps the learning rate is 0.0001 then for the final 5k steps the learning rate is 0.00001.

F.2.1 SAVA

SAVA has remarkably few design choices in comparison to other data pruning methods like EL2N Appendix F.2.2 and supervised prototypes Appendix F.2.3. We train a ResNet18 encoder using the clean training set of size 47,570. Note we do not use this training set to obtain final accuracies in Figure 4, we only use the large noisy training set for obtaining the results in Figure 4. We use a batch size of 2048 for valuation and we use label-2-label matrix caching Appendix G.

F.2.2 EL2N

To obtain values for the points in our noisy training set to then decide which training points to prune, we obtain our *EL2N* scores by training for 10 epochs 10 separate ResNet18 models on the clean training set of size 47,570.

We also hyperparameter optimize the offset $\in \{0.0, 0.05, 0.1\}$ using a sliding window which covers 90% of points §4 (Paul et al., 2021). This is to decide which range of ranked values to keep/ prune. We find that using an offset of 0.0 worked best, so high values of the *EL2N* score will get pruned.

Algorithm 2 Incremental learning experimental setup.

Input: noisy training dataset initially empty $\mathbb{D}_t := \emptyset$ and clean validation set \mathbb{D}_v , data pruning proportion $p \in [0, 1]$.

Output: trained model \mathcal{M} .

```
for  $\mathcal{T}_t = 1, \dots, T$  do
  Get new data  $\mathbb{D}_{\mathcal{T}_t}$ .
  Merge  $\mathbb{D}_{\mathcal{T}_t}$  with existing dataset  $\mathbb{D}_t := \mathbb{D}_t \cup \mathbb{D}_{\mathcal{T}_t}$ .
  Get valuation scores for  $\mathbb{D}_t$  by comparing to  $\mathbb{D}_v$ .
  Prune a proportion  $p$  with the highest data values:  $\tilde{\mathbb{D}}_t$ .
  Train model  $\mathcal{M}$  on  $\tilde{\mathbb{D}}_t$  and evaluate  $\mathcal{M}$  on  $\mathbb{D}_v$ .
```

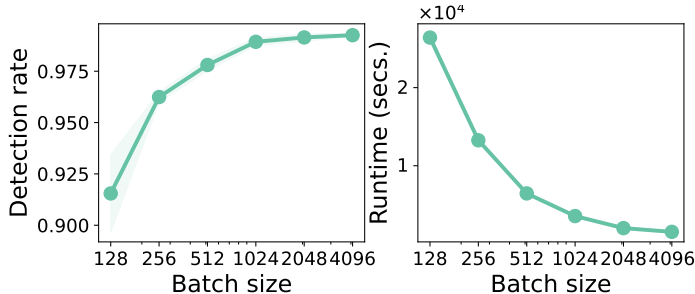


Figure 8: **SAVA performance as function of the batch size, N_i .** The CIFAR10 dataset with noisy label detection. Left: Detection rate. Right: detection runtimes in seconds.

F.2.3 Supervised Prototypes

We train an image encoder using a classification objective on the clean training set provided in the Clothing1M dataset of size 47,570. Note, that we do not use this dataset to train to augment the pruned noisy training sets after valuation and so are not used for the results in Figure 4.

We use mini-batch K-means clustering to obtain centroids for our image embeddings. We tune the mini-batch K-means learning rate over the grid $\{0.1, 0.05, 0.01, 0.005, 0.001\}$ and the number of centroids over the grid $\{1,000, 2,000, 5,000, 10,000\}$ using the intra cluster mean-squared error on the validation dataset.

The best configuration uses a k-means clustering learning rate of 0.05 and 10,000 cluster centers. Then we can obtain cosine distances between every data point and its assigned cluster center and prune points which look the most prototypical before training a classifier on the pruned dataset.

Appendix G Additional Experiments

G.1 Incremental learning

We split the CIFAR10 dataset into 5 equally sized partitions with all classes, and we incrementally build up the dataset such that it grows in size as one would train a production system (Baby et al., 2022). We inject the data with noisy labels and noisy feature corruptions, then perform the data valuation. We compare our proposed method with LAVA (Just et al., 2023). After valuing our training set which is incrementally updated and grows in size throughout the incremental learning, we greedily discard 30% of the data that are the most dissimilar to the validation set and train on the pruned dataset. We report the final accuracy of a ResNet18 (He et al., 2016) model. We summarize this experimental setup in Algorithm 2.

G.2 Performance as a function of batch size

Following the discussion on the batch size in Section 4, we measure our model performance w.r.t. different batch sizes $N_i \in \{128, 256, \dots, 4,096\}$. We show that the performance converges with increasing batch sizes. In this particular setting, the batch sizes of 1,024, 2,048, and 4,096 will

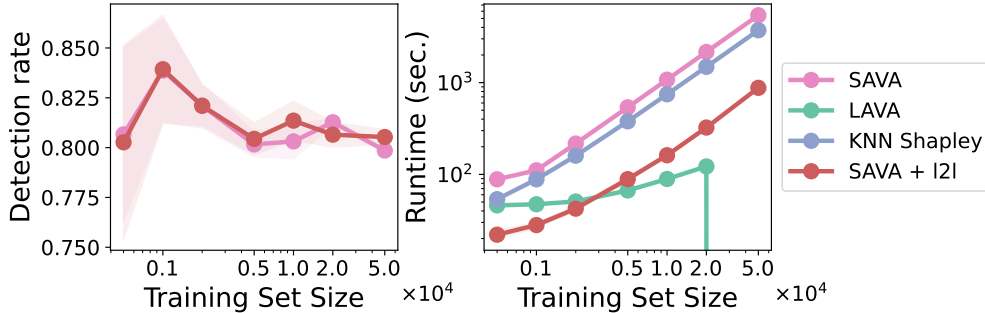


Figure 9: **Label-to-label matrix caching significantly reduces runtime.** Left: *SAVA* with and without label-2-label (I2I) matrix caching performs similarly in detecting noisy label corruption. Right: *SAVA* with I2I runs significantly quicker and is quicker than *LAVA* in terms of runtime in seconds on the same GPU.

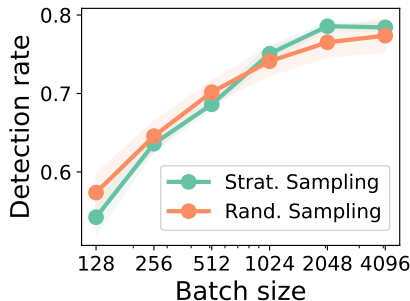


Figure 10: **Randomly sampling data for batch construction is robust.** Detection rates for *SAVA* for random sampling to construct a batch versus stratified sampling which evenly samples data from different classes. The detection rates are calculated after valuation by inspecting the fraction of corrupted data for a prefix of size $N/4$ for CIFAR10 with noisy features.

perform comparably in terms of detection rate while the batch size of 4,096 will consume less time for computation of the cost across batches, since there are less and K_t is lower.

G.3 Label-to-label distance caching

We study the difference in performance and runtime between *SAVA* Algorithm 1 and using *SAVA* with label-to-label (I2I) matrix caching discussed in Section 4 using CIFAR10 with noisy label corruptions. We show that there are almost identical detection rates between the two variants of *SAVA* with and without I2I caching Figure 9. Meanwhile, the runtime is significantly reduced and is lower than *LAVA*.

G.4 Constructing batches

We explore two options for constructing the batches including random sampling and stratified sampling in Figure 10. Since (uniformly) random sampling could result in a batch with an uneven distribution of classes, this could degrade the calculation of the class-wise Wasserstein distance Eq. (1). To mitigate, against any imbalance we compare random sampling versus stratified sampling which evenly samples from each class to construct a batch. When valuing 10k points from the CIFAR10 dataset with corrupted features, we find little difference in detection rates between these two sampling schemes. This might be a consideration when the ratio of the number of classes in the dataset to the batch size is higher.

G.5 On the robustness of Batch-wise LAVA

From the corruption detection experiments, we established that *Batch-wise LAVA* has remarkable performance section 5.1. However, as we vary the batch-size we notice that for small batch-sizes

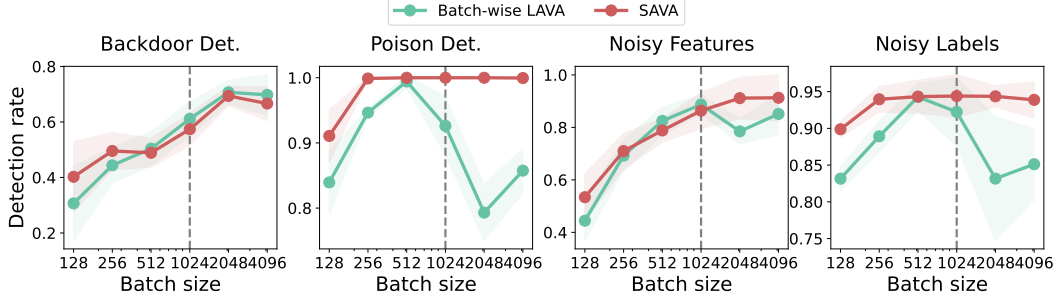


Figure 11: *Batch-wise LAVA is not robust to different batchsizes.* For 4 different corruptions on a training dataset of size 5k with validation dataset size 2k we measure the detection rate for varying batch sizes for *SAVA* and *Batch-wise LAVA*. The dashed grey line centered on 1024 denotes the batch size used in Figure 2.

and large batch-sizes *Batch-wise LAVA* performance deteriorates dramatically Figure 11. For small batches this is due to *Batch-wise LAVA* not having enough clean points in the validation batch to detect corrupt data points in the training batch. For large batches the final batch in the dataloader is usually smaller than the specified batch-size and so these data points in the final batch will also suffer from not enough points in the validation batch to compare against. *SAVA* is able to overcome this issue since the information from all batches is aggregated and weighted by the optimal plan between batches, $\pi_{ij}^*(\bar{\mu}_t, \bar{\mu}_v)$, in lines 7 and 10 in Algorithm 1.

Appendix H Related Works

Data valuation. A simple way to value a datapoint is through the leave-out-out (LOO) error; i.e. the change in performance when the point is omitted, this is inefficient to perform in practice. A more efficient way to value data is through the use of Shapley values with a KNN proxy model (Jia et al., 2019a,b). Extensions of the Shapley value for data valuation include Data Shapley (Ghorbani and Zou, 2019) and Beta Shapley (Kwon and Zou, 2022). Instead of using the Shapley value one can use “the core” from the game theory literature for data valuation (Yan and Procaccia, 2021). An entire dataset can be valued by its diversity, practically this can be done by assessing its volume: the determinant of the left Gram (Xu et al., 2021). An initialized model can also be utilized for data valuation where sets are available from contributors (Wu et al., 2022). The Banzhaf value can also be used for data valuation (Wang and Jia, 2022). Influence functions (Koh and Liang, 2017) approximate LOO retraining using expensive approximations of the Hessian of the NN weights. In a similar vein, TracIn (Pruthi et al., 2020) traces the influence of a training point on a test point by looking at the difference in the loss throughout training. Our approach builds upon *LAVA* which uses the gradient OT distance between the validation and training sets to assign a value to training points (Just et al., 2023). The OpenDataVal benchmark is available with many implementations of data valuation methods (Jiang et al., 2023).

Active learning. Active learning is characterized by selecting points from an unlabeled pool of data for labeling and then using the newly labeled datapoint to update a model (Settles, 2009). Active learning is related to data valuation since a notion of importance is needed to value unlabeled points to then select a label. Unlabeled samples can be valued by using the prediction disagreement from a probabilistic model (Houlsby et al., 2011), this disagreement can also be obtained from multiple models (Freund et al., 1997). This approach of using the disagreement of a probabilistic model can also be thought of as selecting points to label which are the most uncertain via the predictive entropy using probabilistic neural networks (Gal et al., 2017; Kirsch et al., 2019). Alternatively picking points to label can be thought of as a summarization problem by obtaining a coresets of representative data (Sener and Savarese, 2018; Mirzasoleiman et al., 2020; Coleman et al., 2019). Samples to be labeled can be selected by interpreting the classifier output probabilities as a confidence (Li and Sethi, 2006).

Data selection. Active learning is used to select points to label and so its importance metric doesn’t use label information, however, it has been shown to achieve competitive results for data selection; speeding up the generalization curve over the course of training (Park et al., 2022). The influence

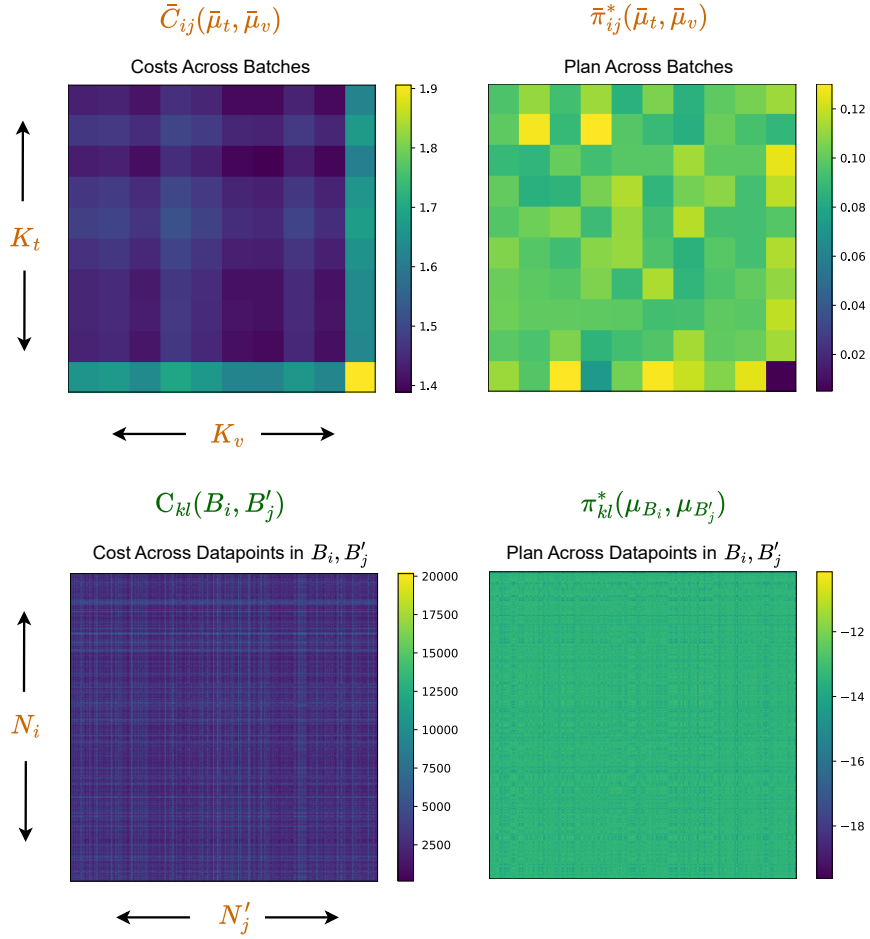


Figure 12: **Visualization of the main artifacts in Algorithm 1.** For a noisy CIFAR10 valuation problem with a training and validation set size of 10k and SAVA batch size of 1024, we visualize the main artifacts of the SAVA algorithm for illustrative purposes. From left to right, from the top row to the bottom row: the first matrix is the cost matrix between batches: $\bar{C}(\bar{\mu}_t, \bar{\mu}_v)$ and then the optimal plan $\bar{\pi}^*(\bar{\mu}_t, \bar{\mu}_v)$ is the associated plan which is the solution to the optimal transport problem. In the second row we visualize $C(\mu_{B_i}, \mu_{B'_j})$ the optimal transport distance between points in the final batch B_i from the training set and the final batch B'_j in the validation set and its corresponding optimal plan $\pi^*(\mu_{B_i}, \mu_{B'_j})$, we have used a log transform to on the optimal plan between datapoints to help viewing it.

a point has on the training loss as a metric of informativeness has been shown to accelerate the training of neural networks (Loshchilov and Hutter, 2015). Similarly picking points that reduce the variance of the gradient speeds up training (Katharopoulos and Fleuret, 2018; Johnson and Guestrin, 2018). Instead of focusing on the training loss, one can select data according to the influence on the validation loss (Mindermann et al., 2022). Instead of selecting data to train on, one can equivalently prune away uninformative data. The data’s contribution of the gradient norm of the loss with respect to model parameters is a natural measure for deciding which datapoints to prune from a dataset (Paul et al., 2021). One can also prune data by how similar embeddings are to a cluster center or prototype (Sorscher et al., 2022) and by assessing diversity within each cluster (Abbas et al., 2023; Tirumala et al., 2023). It has also been shown that pruning data according to how easy they are to be forgotten over the course of training - as a measure of difficulty - results in training on less data while maintaining performance (Toneva et al., 2018). These data selection methods although related, do not directly measure the importance of each training datapoint with respect to a clean validation set like *LAVA* (Just et al., 2023) and *SAVA*. Meta-learning is also used to learn datapoint importance weights by evaluating with a clean validation set (Ren et al., 2018). Similarly to *LAVA* and *SAVA* the distributional distance between a clean validation set and a large noisy dataset can be assessed using n-grams in NLP for selecting data to train large language models (Xie et al., 2023).

Appendix I SAVA Visualization

To gain insight into how the estimated OT matrices from our proposed *SAVA*, we visualize the artifacts Algorithm 1 in Figure 12.

Appendix J Other Discussions

Overfitting and Approximation. Recently, Peyré and Cuturi (2019, §8.4) revealed an important property that solving exactly the OT problem may lead to overfitting. Therefore, investing excessive efforts to compute OT exactly would not only be expensive but also self-defeating since it would lead to overfitting within the computation of OT itself. As a result, our batch approximation can be considered as a regularization for OT. We show empirically for certain cases that the batch approximation (*SAVA*) performs better than the original OT (*LAVA*) in terms of quality while we surpass *LAVA* in memory requirement.